scientific reports

OPEN

Biodistribution of PET radiotracers in tumor-bearing TRAMP mice administered by retroorbital or jugular vein injections

Catherine C. Applegate[1,2,3✉], Michael B. Nelappana[1,2], Yuxiao Cui[1,3], Goodluck Okoro[1], Elaine A. Nielsen[1], Nicolas P. Dovalovsky[1], Andrew M. Smith[1,3,4,5,6], Iwona T. Dobrucki[1,2,5,7] & Lawrence W. Dobrucki[1,2,5,6,8]

Nuclear medicine is an important tool for use in molecular imaging of important biological processes. Methods for intravenous delivery of radiotracers remains a challenge, with tail vein injections demonstrated to be technically difficult and lacking in reproducibility. Other intravenous methods include jugular vein (JV) injection, which requires a more invasive and precise microsurgical technique. Although the retroorbital (RO) sinus drains directly into the JV, and RO injections are minimally invasive and simpler to perform, they remain underutilized, perhaps due to a lack of studies demonstrating their performance. This study provides a comprehensive comparison of dynamic tissue biodistribution of three categories of commonly utilized radiopharmaceuticals between JV and RO injection methods in prostate tumor-bearing mice using PET-CT imaging. Results show that JV and RO injections have equivalent dynamic tissue biodistributions across the three categories of radiopharmaceuticals used: (1) small molecule measuring tumor metabolism (^{18}F-flurodeoxyglucose [FDG]); (2) peptide-based probe measuring angiogenesis (^{64}Cu-NOTA-PEG$_4$-cRGD$_2$); and (3) dextran-based nanocarrier (^{64}Cu-NOTA-D20). Although RO injections present with some limitations such as type of injectate and difficulty for measuring acute, dynamic pharmacokinetics, this study demonstrates that RO injections are a viable, minimally invasive or stressful, and efficient alternative intravenous delivery technique for molecular imaging.

Molecular imaging is a useful tool for non-invasively visualizing, characterizing, and quantifying molecular processes that occur at cellular or subcellular levels within a living organism. Molecular imaging involves various modalities ranging from standard methods such as the application of nuclear medicine and MRI to more basic methods such as photoacoustic and Raman microspectroscopy[1]. Molecular imaging modalities applied in nuclear medicine, which involves the delivery of molecular tracers labeled with radioactive tags to the organism, rely on the identification of biological abnormalities, such as cancers, and correlation of anatomical structures through the combined use of high spatial resolution computed tomography (CT) and high sensitivity positron emission tomography (PET) imaging[2]. Based off the radioactive signal emitted from tissues detected by PET and spatially localized through CT, researchers and clinicians can visualize areas of the body with increased signal.

Delivery methods for radiotracers can be different depending on the region of interest (ROI); however, most imaging techniques aimed at detecting cancers involve intravenous delivery. In small animal research involving murine models, tail vein injections are commonly used for intravenous access. Unfortunately, tail vein injections

[1]Department of Bioengineering, University of Illinois at Urbana–Champaign, 405 N. Mathews Ave, MC-251, Urbana, IL 61801, USA. [2]Beckman Institute for Advanced Science and Technology, University of Illinois at Urbana–Champaign, Urbana, IL 61801, USA. [3]Micro and Nanotechnology Laboratory, University of Illinois at Urbana–Champaign, Urbana, IL 61801, USA. [4]Department of Materials Science and Engineering, University of Illinois at Urbana–Champaign, Urbana, IL 61801, USA. [5]Department of Biomedical and Translational Sciences, Carle-Illinois College of Medicine, University of Illinois at Urbana-Champaign, Urbana, IL 61853, USA. [6]Cancer Center at Illinois, University of Illinois at Urbana-Champaign, Urbana, IL 61801, USA. [7]Academy of Medical and Social Applied Sciences, Elblag, Poland. [8]Division of Medical Laboratory Diagnostics - Fahrenheit Biobank BBMRI.pl, Medical University of Gdansk, Gdansk, Poland. ✉email: cca2@illinois.edu

are oftentimes stressful to the animal, technically difficult, non-reproducible, and not sustainable for multiple injections over time[3]. Tail vein injections delivered as a bolus are also delayed in reaching circulation above the diaphragm due to the limited diameter of the inferior vena cava, resulting in a slower and more sustained distribution[4]. A common alternative to tail vein injections is by direct injection into the jugular vein (JV). However, JV injections require specialized equipment and microsurgical experience, result in increased animal stress and potentially loss, carry risk for infection, and are limited for multiple injections over time. Additionally, for both tail vein and JV methods, extravasation is common, resulting in the reduced ability to adequately quantify the true dose delivered[5,6].

The retroorbital (RO) sinus vein is an under-utilized intravenous access point that allows for reproducible and repeatable injections that are less invasive, less stressful, and technically simpler to perform compared with tail vein or JV methods. Inadequate radiotracer delivery or severe extravasation is easily apparent while performing RO injections, thus limiting potential errors in biodistribution calculations based on incomplete dose delivered. Several studies have compared the biodistribution of substances delivered via tail vein or RO injections and have found no significant differences in overall tissue uptake following either method[3,4,7–9]. Fewer studies have compared JV and RO methods, with results similarly demonstrating no significant differences in overall probe biodistribution[3,10].

Specific to molecular imaging in cancer research, the category of probe and the resulting tumor uptake are important factors to consider when selecting an appropriate intravenous delivery method. The small molecule radiotracer, ^{18}F-flurodeoxyglucose (FDG), has been revolutionary in PET imaging and is widely utilized for cancer diagnoses and monitoring[11]. For additional functional and physiological information as well as therapeutic effects, several peptide-based radiotracers are established for clinical theranostic use for multiple types of cancers owing to their efficient tumor targeting capabilities[12]. However, peptide size contributes to low blood circulation time, which decreases therapeutic efficacy. As such, tunable nanoparticles are being widely explored for theranostic use in nuclear medicine, as nanoparticles offer the advantages of targeting efficiency, length of exposure, increased tumor accumulation through the enhanced permeability and retention (EPR) effect, and high drug carrying capacity[12]. To date, no studies have compared tissue-specific dynamic and overall biodistribution of multiple probe categories commonly used and studied for use in cancers and administered by different intravenous methods in a tumor-bearing murine model. The goal of this study was to provide a comprehensive comparison between JV with RO injection methods delivered to a cancer-bearing mouse model across three categories of radiopharmaceuticals (small molecule, peptide, and nanoparticle) commonly utilized in both clinical and preclinical cancer research, measured using small-animal micro-PET-CT: (1) small molecule measuring tumor metabolism (^{18}FDG); (2) peptide-based probe binding to $\alpha_v\beta_3$ integrin, a well-characterized biomarker for angiogenesis (^{64}Cu-NOTA-PEG4-cRGD$_2$, developed by our group)[13]; and (3) dextran-based nanocarrier developed by our group (^{64}Cu-NOTA-D20)[14]. The transgenic adenocarcinoma of the mouse prostate (TRAMP) model was selected as an immunocompetent orthotopic mouse model of spontaneous prostate cancer, which is commonly measured and treated using these types of radiotracers[15].

Methods and materials
Animals and tumor detection
All animal procedures were approved by the Institutional Animal Care and Use Committee (IACUC) at the University of Illinois at Urbana-Champaign, and all procedures were carried out in accordance with both IACUC guidelines and the ARRIVE guidelines for vertebrate animal experiments. Male C57Bl/6-Tg(TRAMP)8247Ng/J mice were purchased from The Jackson Laboratory (Bar Harbor, ME, USA). Upon arrival, mice were housed in groups of four in standard shoebox cages (452 cm^2) and fed standard chow diet (Teklad Global; ENVIGO, Madison, WI) under a temperature- and humidity-controlled environment, with a 12 h light-12 h dark cycle.

Prostate tumor development was monitored bi-weekly via ultrasound imaging (VisualSonics Vevo 2100, Toronto, Canada) starting at 10 weeks of age until tumor detection. Briefly, mice were anesthetized and maintained under 2% isoflurane (or to effect) in 1–2 L/min O$_2$. Hair over the lower abdomen was removed by a standard commercial depilatory agent, and ultrasonic scans were obtained in 3D B-mode through the ventral body wall while animals laid in dorsal recumbency on a heated table. Upon tumor detection, mice were randomized to receive either JV or RO injections.

Radiolabeling of cRGD$_2$ peptide-based tracer
A stock solution of $^{64}CuCl_2$ (Washington University, St. Louis, MO) was diluted to a final volume of 100 µL using ammonium acetate buffer (0.1 M, pH 5.5). To prepare the buffer, 1.03 mL of glacial acetic acid and 7.7 g of ammonium acetate were added to 995 mL of double-distilled, sterile water, and the pH was adjusted to 5.5. The buffer was treated with 10 g of Chelex 100 resin (Bio-Rad Laboratories, CA, USA) overnight to remove free metal ions, followed by vacuum filtration to remove the resin.

For radiolabeling, 500 µL of the ammonium acetate buffer was added to a vial containing 25 µg of NOTA-PEG$_4$-cRGD$_2$, which is a dimeric peptide-based probe developed by our lab that targets $\alpha_v\beta_3$ to measure angiogenesis.[13] The radiolabeling protocol developed by our lab has been previously described and shown to result in chemical stability and a radiochemical purity of ≥ 95% as measured by HPLC and TLC[13]. Briefly, the vial was vortexed to dissolve the tracer and then placed on a shaker at 800 rpm for 15 min at room temperature. The air was evacuated from the vial using a syringe, and the desired activity of the $^{64}CuCl_2$ stock solution (≤ 74 MBq) was added. The mixture was vortexed again and placed on the shaker for an additional 15–30 min to allow ^{64}Cu binding. The radiolabeled product in the prepared buffer was then ready for dose aliquots to be administered immediately.

Synthesis and radiolabeling of Dextran 20 (D20)-NOTA nanoparticle

This synthesis and labeling method is consistent with previous protocols used in our lab for Dextran 500[16]. Typically, Amino-Dextran 20 (10 mg, 10 NH2/Dextran 20; Fina Biosolutions, Rockville, MD) was dissolved in 5 mL of anhydrous DMSO (Sigma-Aldrich, St. Louis, MO) under a nitrogen atmosphere in a 25 mL Schlenk flask. Triethylamine (10 µL; Sigma-Aldrich) was added, and the mixture was stirred for 10 min. p-SCN-Bn-NOTA (7 mg, 12.5 µmol; Macrocyclics, Plano, TX) dissolved in 1 mL of anhydrous DMSO was added dropwise. The reaction proceeded for 14 h, and the product was transferred to a dialysis bag (MWCO 1 kDa; Spectrum Labs, Rockleigh, NJ) and dialyzed against 3.5 L of deionized water for 24 h. The final product, D20-NOTA, was obtained as a white solid after lyophilization and confirmed by ^1H NMR.

For radiolabeling, 500 µL of D20-NOTA (1 mg/mL) in 0.1 M pH 5.5 ammonium acetate buffer was mixed with 40.7 MBq of $^{64}CuCl_2$. The mixture was incubated at 37 °C with shaking at 800 rpm for 30 min. Cold copper (twofold molar excess to NOTA; Sigma-Aldrich) was added, and the reaction continued for another 20 min. EDTA (twofold molar excess to copper) was then added and incubated for 15 min at 37 °C to sequester free copper. The solution was filtered using an Amicon filter (MWCO 3 kDa; MilliporeSigma, Urbana, IL) with three washes: the first with 0.1 M pH 5.5 ammonium acetate buffer, and the subsequent two with saline. The final product, with a radiochemical purity exceeding 95% (Supplemental Fig. S1), was verified using radio-thin layer chromatography (radio-TLC) with an ethanol and ammonium acetate mobile phase (1:1 v/v).

Jugular vein (JV) injection

Animals were anesthetized and maintained with 1–3% isoflurane in 1–2 L/min O_2 and administered analgesic (Carprofen, 5 mg/kg) subcutaneously. Depth of anesthesia was monitored by pedal reflex and respiratory rate. The neck and chest were shaved using a small animal shaver prior to treatment with a commercial depilatory agent for ~ 3 min followed by swabbing with dampened gauze. The skin was then sterilized using povidone-iodine solution prior to surgical procedure, and animals were placed under a surgical microscope. A small incision (~ 10 mm) was made in the neck above of the manubrium and to the side of the trachea to find and expose the external JV. The vein was carefully separated from the nearby tissue and gently stretched using forceps before a dose of approximately 3.7 MBq of ^{64}Cu-NOTA-PEG4-cRGD$_2$ or ^{64}Cu-NOTA-D20 or approximately 6.5 MBq ^{18}F-FDG (PETNET Solutions, Chicago, IL) in ≤ 100 µL was injected using a 31-gauge insulin syringe, taking care to keep the needle parallel with the vein and prevent puncture through the vein and off-target injection.

Gentle pressure was applied using a sterile cotton-tipped applicator to press down on the vein and surrounding tissue for 30 s or until any resultant bleeding from the injection ceased, and mice were immediately transferred to the PET-CT for imaging. Following dynamic PET-CT imaging, the surgical incision in the skin was then sutured using size 6–0 silk sutures and the surgical site was swabbed with povidone-iodine solution.

After imaging, animals were placed in a clean cage and monitored during recovery and for 12 h post-surgery for any discomfort. Seven to ten days post-surgery, sutures were removed under light anesthesia.

Retroorbital (RO) injection

Animals receiving RO injections were anesthetized as described. Prior to performing the RO injection, a drop of analgesic bupivacaine HCl (Alcon Laboratories, Inc., Fort Worth, TX) was administered to the eye. The mouse was briefly removed from the anesthesia nose cone and placed in lateral recumbency. The mouse's eyeball was then carefully protruded from the eye socket by applying gentle pressure to the skin dorsal and ventral to the eye. A 28-gauge, 0.5 in insulin needle with ≤ 100 µL injectate was carefully introduced at an angle of approximately 30°, bevel down, into the medial canthus. The needle followed the edge of the underside of the eyeball down until the needle tip was at the base of the eye, often indicated by the tip of the needle touching an orbital bone. The radiotracer was injected into the RO sinus vein, the needle was slowly withdrawn, and mice were transferred to the PET-CT for imaging.

Dynamic PET-CT

Serial, dynamic in vivo PET-CT imaging was performed immediately following radiotracer administration in animals assigned to either JV or RO groups for a total of 3 imaging sessions per animal over a 2-week period. A timer was used to record the time between injection and the start of imaging to ensure accurate radio decay-correction and time-course comparisons. Animals were placed in a supine position on the polyacrylic imaging bed of a small animal-dedicated micro-PET-CT scanner (Inveon, Siemens Healthcare, Erlangen, Germany). Animals underwent 30 min dynamic PET imaging (15% energy window centered at 511 keV) followed by anatomical X-ray CT imaging (80 keV, 500 µA, 100 µm spatial resolution).

The functional PET and anatomic CT images were reconstructed using the OSEM/3D and cone-beam algorithms, respectively. Three-dimensional ROIs of 100 µm thickness were drawn manually around tissues of interest using the CT images to generate kinetic tissue activity curves, taking care to select consistent regions between animals. ROIs were drawn around the whole tumor to account for intratumoral heterogeneity of probe uptake.

Statistical analysis

Statistical analysis was performed using GraphPad Prism (GraphPad Prism Software v.10.0.2, San Diego, CA). Data are presented as mean ± standard error of the mean (SEM) and expressed as percentage of injected dose per gram tissue (%I.D./g). For PET-CT analysis of average tissue uptake, unpaired two-tailed Student's t-test was used to determine significance between JV and RO administration groups. For dynamic PET-CT analysis, a repeated measures two-way ANOVA with time, injection type, and their interaction was used to determine significance, followed by Tukey's post-hoc analysis. A p-value < 0.05 was considered significant.

Results

A schematic diagram depicting the chemical structures of each radiopharmaceutical is shown in Fig. 1. Prostate tumor-bearing TRAMP animals were randomized to receive JV or RO injections of ^{18}F-FDG, ^{64}Cu-NOTA-PEG$_4$-cRGD$_2$, or ^{64}Cu-NOTA-D20 radiotracers (n = 3/group; Fig. 2A) over the course of 2 weeks. Schematics depicting JV and RO injection methods are shown in Fig. 2B and Fig. 2C, respectively. Dynamic PET images acquired over 30 min were initiated between 2–3 min post-injection for all radiotracers with subsequent anatomical colocalization acquired by CT imaging.

Tissue-specific uptake of small molecule probe: ^{18}F-FDG

The average time from ^{18}F-FDG radiotracer injection to start of PET imaging was 2 min, 38 s. Average tissue-specific uptake were not different between injection methods for kidney, spleen, lung, or liver (Fig. 3A). Blood
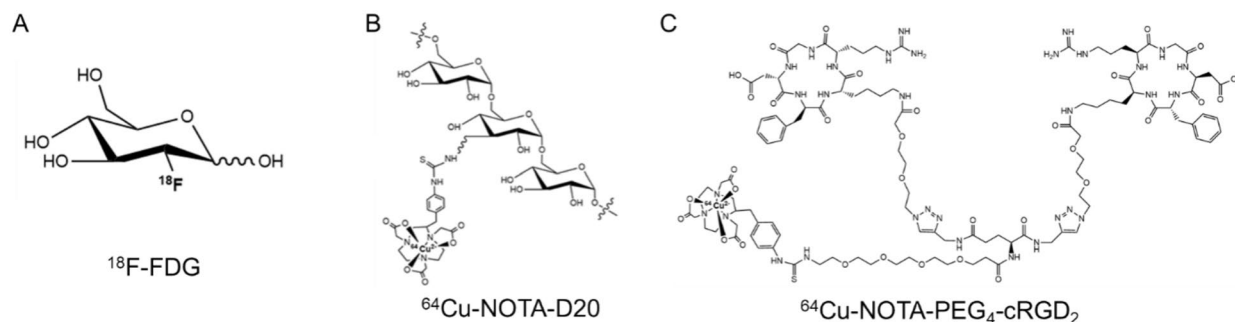
Fig. 1. Schematics of radiotracers. (**A**) Small molecule-based probe ^{18}F-fluorodeoxyglucose (FDG); (**B**) nanoparticle-based probe ^{64}Cu-NOTA-Dextran 20 (D20); and (**C**) peptide-based probe ^{64}Cu-NOTA-PEG$_4$-cRGD$_2$.
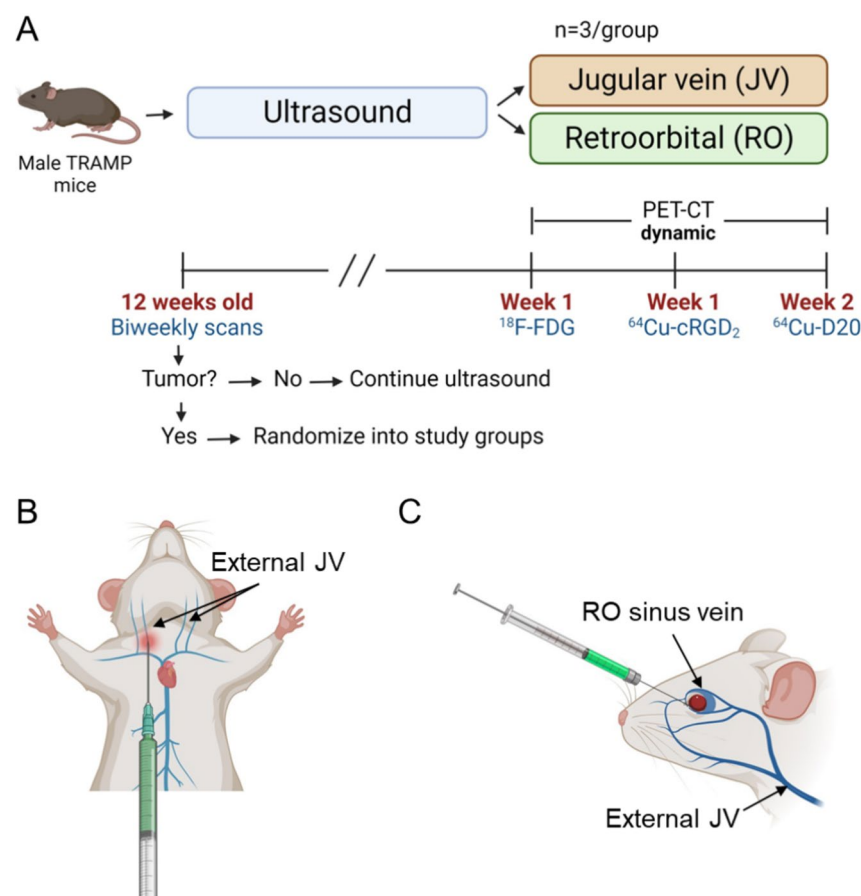
Fig. 2. Study design and injection methods. (**A**) Study design using prostate tumor-bearing transgenic adenocarcinoma of the mouse prostate (TRAMP) mice. Schematics depicting anatomical location of (**B**) jugular vein (JV) and (**C**) retroorbital (RO) injection methods.
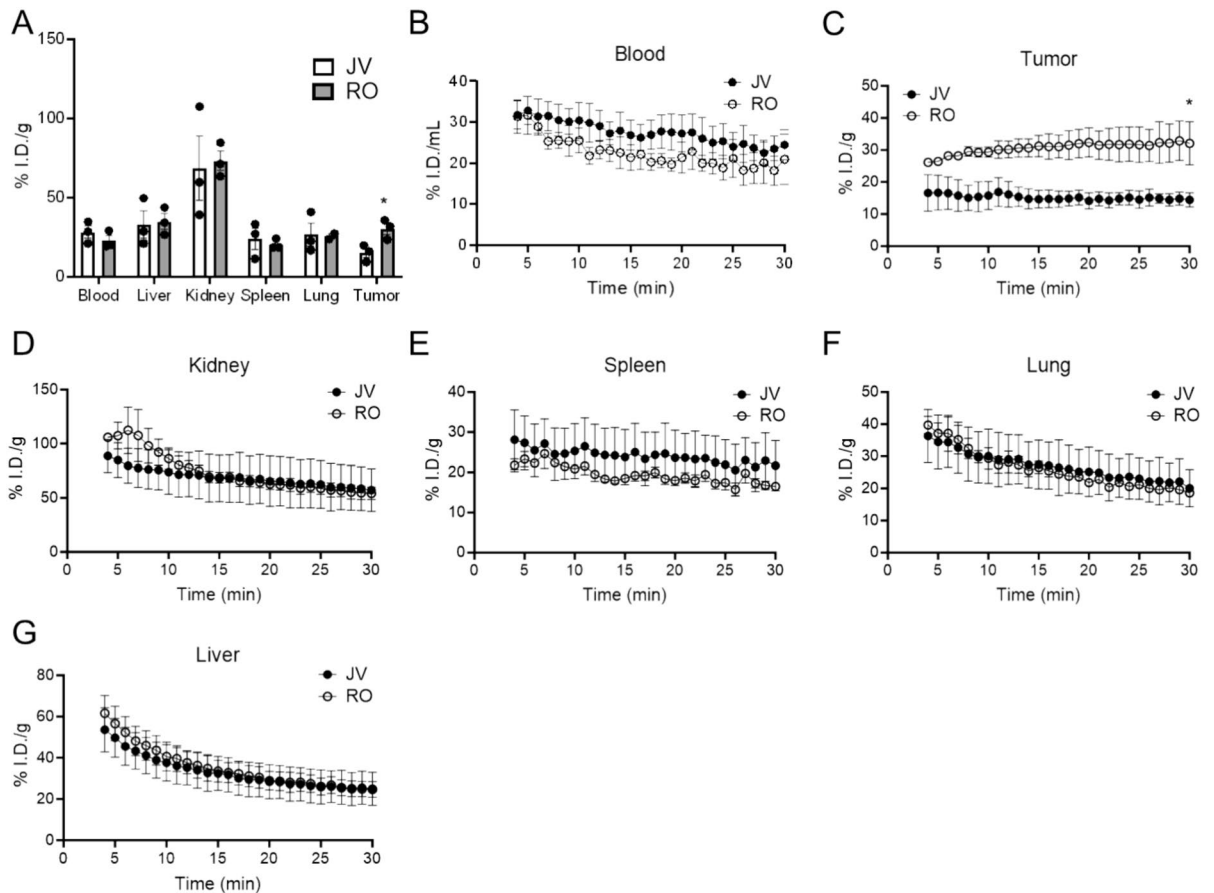
Fig. 3. Dynamic PET quantification following ^{18}F-FDG injection. (**A**) Average tissue uptake demonstrates significant differences in tumor uptake following JV injection due to variations in tumor biology between individual animals. (**B**) Blood levels demonstrate consistent circulation of FDG over time. Time-dependent biodistribution demonstrates differences in (**C**) tumor uptake but equivalent probe uptake in normal tissues: (**D**) kidney; (**E**) spleen; (**F**) lung; and (**G**) liver. Data are shown as mean $\pm$ SEM (*$p < 0.05$ by Students' t-test or two-way ANOVA with Tukey's *post-hoc*; $n = 3$/group).

values were measured to demonstrate equivalent circulation of each probe and were found to demonstrate similar blood circulation, indicating complete injectate administration by each method. Average tumor uptake was significantly different between injection methods, with overall tumor tissue uptake greater following RO compared with JV injection ($p = 0.033$).

Consistent with average values, tumor uptake of ^{18}F-FDG was significantly increased following RO injections at all timepoints as measured by dynamic PET over time within CT-identified ROIs (Fig. 3C, p = 0.029). While tumor uptake results suggest inefficient JV injection or enhanced extravasation following JV injection, equivalent small molecule probe distribution was observed over time in kidney, spleen, lung, and liver between JV and RO injection methods, suggesting efficient probe delivery within each method (Fig. 3D–G). Dynamic PET-CT images were examined for evidence of extravasation following JV injection, but none was observed at any timepoint. As can be seen in Fig. 4, high inter- and intratumor heterogeneity in probe uptake over time was observed, likely due to biological differences in tumor vascularization and metabolic activity of the tumors in each injection group. For example, while homogenous probe uptake was observed in the small tumor of the JV-injected mouse (Fig. 4A), regional differences in tumor uptake of ^{18}F-FDG can be observed following RO injection due to the larger tumor size with highly metabolic outer edges and a hypometabolic necrotic core (Fig. 4A). Despite randomization, animals in the RO injection group presented with tumors with greater metabolic activity compared with tumors from animals in the JV-injected group. These differences are evident by the end of the 30 min scan, by which time ^{18}F-FDG has fully distributed and limited variability in probe uptake can be observed between the two groups compared with the high variability in time-dependent uptake observed at earlier timepoints (Fig. 3C). These biological differences likely would have been minimized with greater sample size and resultant increased statistical power.

### Tissue-specific uptake of peptide-based probe: ^{64}Cu-NOTA-PEG$_4$-cRGD$_2$

The average time from ^{64}Cu-NOTA-PEG$_4$-cRGD$_2$ radiotracer injection to start of PET imaging was 2 min, 44 s. Average blood distribution of the probe and tissue-specific uptake were not different between injection methods for kidney, spleen, lung, or liver (Fig. 5A). Equivalent time-dependent blood distribution is shown in
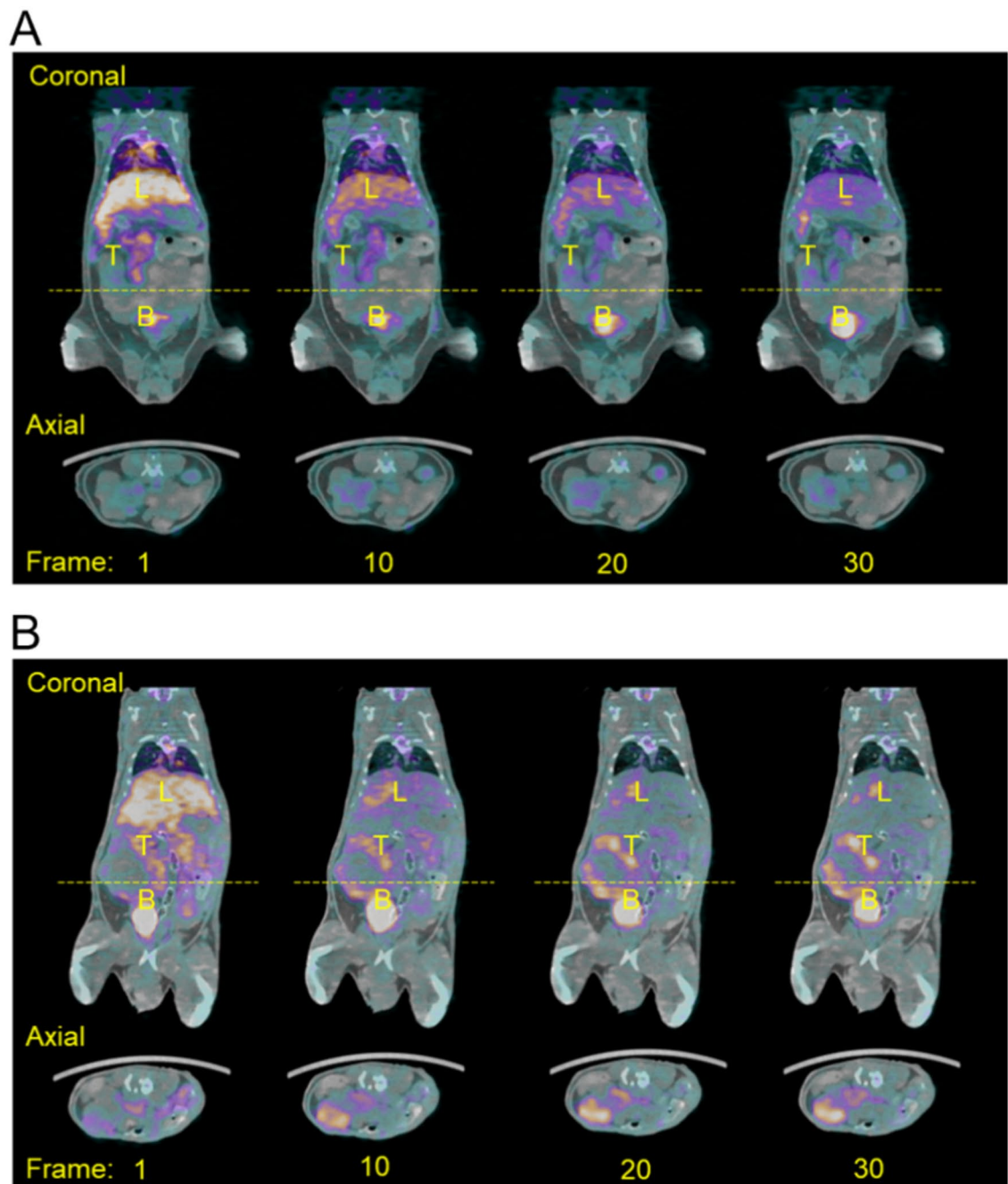
Fig. 4. Representative dynamic PET overlayed on anatomical CT images following ^{18}F-FDG injection. Sequential images at frames (minutes) 1, 10, 20, and 30 via either (**A**) JV or (**B**) RO injection methods are shown. Images demonstrate heterogeneous inter- and intratumoral uptake. Yellow dashed line on coronal view corresponds to slice shown in axial view. *L* liver, *T* tumor, *B* bladder.

Fig. 5B. While average tumor-specific uptake was not significantly different between JV or RO injections, there was a significant time-dependent interaction observed between the two methods (Fig. 5C, p = 0.031). Targeted towards $\alpha_v\beta_3$ integrins, the cRGD$_2$ peptide-based probe accumulates in regions with elevated angiogenesis[13]. Delayed accumulation of ^{64}Cu-NOTA-PEG$_4$-cRGD$_2$ in tumors of animals in the JV injection group indicates reduced angiogenesis occurring in these tumors, results which are consistent with reduced ^{18}F-FDG accumulation observed in this group. Moreover, Fig. 5D–G shows equivalent dynamic peptide-based probe distribution in kidney, liver, lung, and spleen measured over time between JV and RO injection methods. Representative PET-CT images are shown in Fig. 5H. These results demonstrate the biological variations observed between tumors of animals in each injection group.
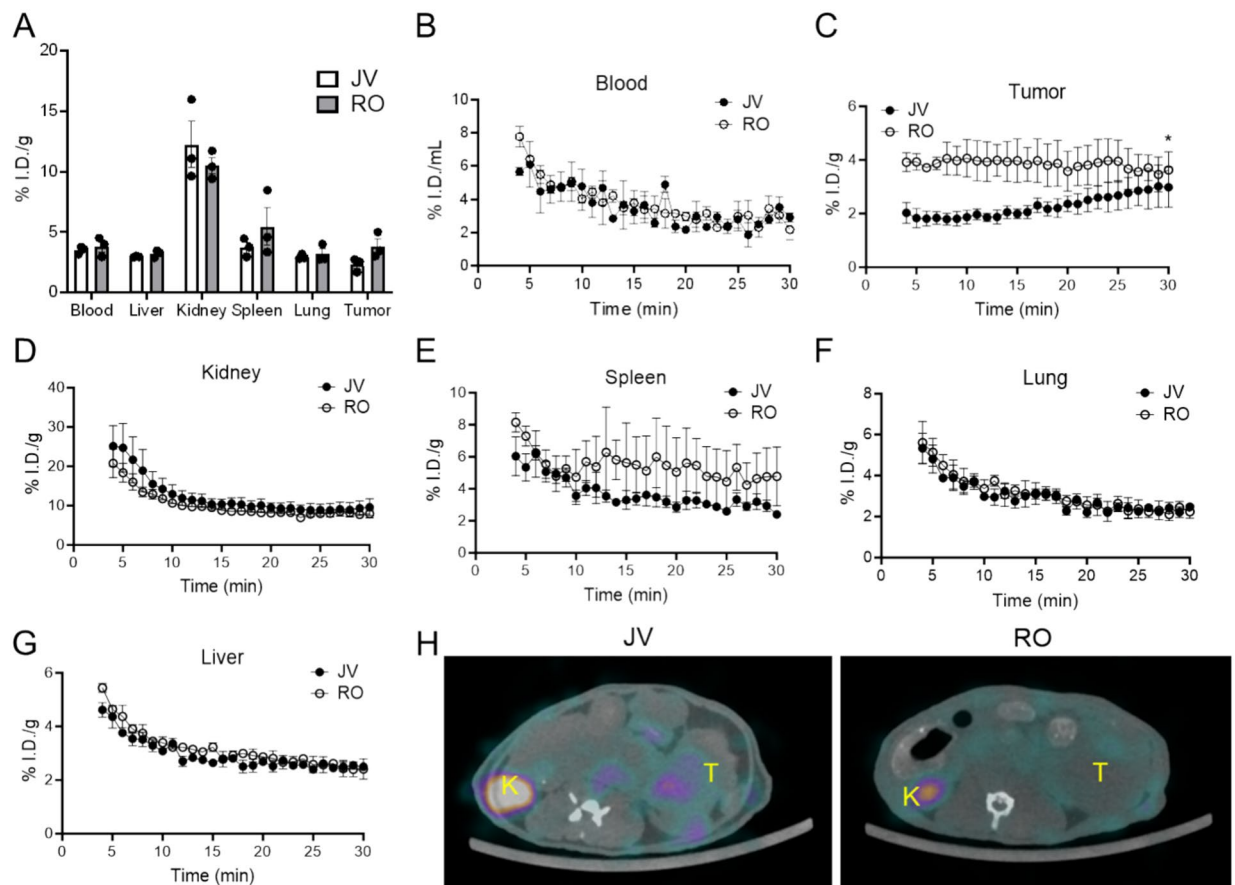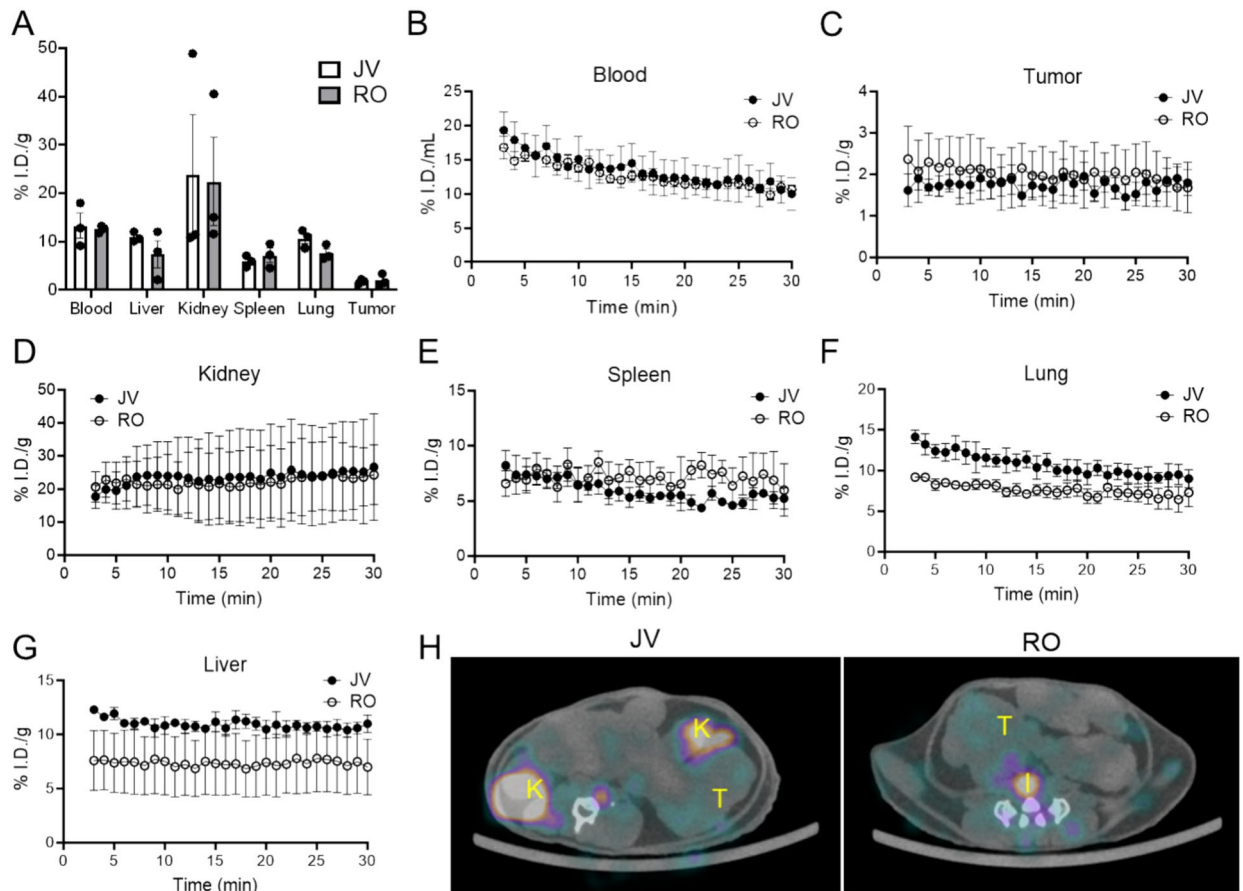
Fig. 5. Dynamic PET quantification following ^{64}Cu-NOTA-PEG$_4$-cRGD$_2$ injection. (**A**) Average tissue measurements demonstrate equivalent probe uptake in all tissues. Time-dependent biodistribution demonstrates equivalent probe (**B**) circulation in blood and uptake in (**C**) tumor; (**D**) kidney; (**E**) spleen; (**F**) lung; and (**G**) liver. (**H**) Representative axial slices of overlayed PET-CT images at 30 min post-JV or RO injection demonstrating inter- and intratumoral heterogeneous probe uptake by prostate tumors (*T* tumor; *K* kidney). Data are shown as mean ± SEM (*$p < 0.05$ by Students' t-test or two-way ANOVA with Tukey's *post-hoc*; $n = 3$/group).

Tissue-specific uptake of nanoparticle-based probe: ^{64}Cu-NOTA-D20

The average time from ^{64}Cu-NOTA-D20 radiotracer injection to start of PET imaging was 2 min, 25 s. Average probe circulation in blood and tissue-specific uptake were not different between injection methods for tumor, kidney, spleen, lung, or liver (Fig. 6A). Similarly, results from dynamic PET quantification demonstrate equivalent nanoparticle-based probe distribution in blood, tumor, kidney, spleen, lung, and liver measured over time between JV and RO injection methods (Fig. 6B–G). Despite biological differences in tumors between JV- and RO-injected mice, tumor uptake of ^{64}Cu-NOTA-D20 was not different between the groups, although heterogeneous intratumoral probe distribution can be observed in representative PET-CT images shown in Fig. 6H. Although dextran nanoparticles have been found to have enhanced tumor permeability compared with small molecule drugs and are rapidly internalized by cells through receptor-mediated endocytosis[17], these data demonstrate reduced uptake of ^{64}Cu-NOTA-D20 in tumor tissues compared with peptide-based ^{64}Cu-NOTA-PEG$_4$-cRGD$_2$. These results suggest equivalent nanoparticle biodistribution into tumors despite differences in metabolism and angiogenesis.

Discussion

This study used PET-CT to examine potential differences in biodistribution of three distinct categories of widely utilized and studied radiotracers between two methods of intravenous delivery (JV or RO) in a cancer-bearing mouse model. We selected the TRAMP model to represent a clinically relevant immunocompetent and orthotopic model of prostate cancer, as prostate cancer is one of the most commonly cancers diagnosed worldwide[18] and for which numerous theranostic radiopharmaceuticals have been developed[15]. Results from this study demonstrate that RO injections provide equivalent in vivo biodistribution of different categories of radiotracers compared to JV injections, indicating RO injections are a suitable, less invasive, and less technically challenging alternative for use in imaging studies involving radiopharmaceuticals. Similar kinetics were observed in all normal tissues following either JV or RO injection, results which are in line with the anatomical features of the RO sinus. The RO sinus is a large space between the back of the eyeball and the orbital bone that contains several branching blood vessels that drain directly into the external JV to make up a substantial amount of JV blood flow (Fig. 2C)[19]. As

Fig. 6. Dynamic PET quantification following ^{64}Cu-NOTA-D20 injection. (**A**) Average tissue measurements demonstrate equivalent probe uptake in all tissues. Time-dependent biodistribution demonstrates equivalent probe (**B**) circulation in blood and uptake in (**C**) tumor; (**D**) kidney; (**E**) spleen; (**F**) lung; and (**G**) liver. (**H**) Representative axial slices of overlayed PET-CT images at 30 min post-JV or RO injection demonstrating inter- and intratumoral heterogeneous probe uptake by prostate tumors (T: tumor; K: kidney; I: intestines). Data are shown as mean ± SEM (*$p < 0.05$ by Students' t-test or two-way ANOVA with Tukey's *post-hoc*; $n = 3$/group).

such, it is not surprising that RO injections result in similar tissue biodistribution compared with intravenous delivery by direct JV injection.

Although kinetic biodistribution patterns were similar in normal tissues across either JV or RO injection methods, it is important to note that dynamic PET scans were initiated between 2–3 min post-injection. In order to measure probe pharmacokinetics, it is essential to quantify probe circulation distribution half-life, which typically occurs during the first few minutes following intravenous administration. For example, the small molecule probe FDG peaks in circulation and distributes to half its concentration within 5 s of cardiac administration[20], reaching a plateau in tissues by 30 min[21]. Larger, peptide-based probe cRGD$_2$ similarly peaks in circulation within seconds of administration and clears from the blood within 5–10 min, plateauing in tissues after 30 min[13]. The distribution half-life is instrumental in determining the elimination half-life of each probe and provides crucial information for creating complete, compartmental pharmacokinetic models. RO injections are limited in measuring pharmacokinetics by the time it takes between injection to the start of dynamic measurement, whereas JV catheterization enables real-time injection measurements.

Catheterization of the targeted vessel is an important tool for measuring the immediate and dynamic pharmacokinetics of the probe in question. While RO catheterization has been described by one group that engineered an appropriate RO catheter[22], this method presents with challenges associated with stabilizing the catheter once it is inserted into the RO sinus. Although technically challenging, JV catheterization enables repeated injections over time for ease of dynamic studies measuring drug or probe pharmacokinetics. In addition to limitations for pharmacokinetic studies, other limitations to RO administration include interference with brain imaging due to enhanced facial and cerebral vein uptake of the injected probe as the facial, brain, and ocular veins all exchange blood freely[19]. By contrast, if targeting the brain is an experimental goal, RO injections may provide an advantage over JV injections for this reason. Cytotoxic substances (e.g. chemotherapies) should also not be delivered by RO injection due to leakage of the injectate from the surrounding veins into delicate ocular and brain tissues[23].

Despite similarities in normal tissue biodistribution of each probe, differences in tumor uptake over time for small molecule probe FDG (metabolism) and molecularly targeted, peptide-based probe cRGD$_2$ (angiogenesis) between injection methods were apparent. Analyses of dynamic PET data provide evidence that injections were

performed efficiently and that differences in tumor uptake were not due to injection method but were rather due to heterogeneous tumor biology between animals from each group. Despite randomization, tumors of JV-injected animals were less metabolically active and less active angiogenesis compared with tumors from RO-injected animals, demonstrating reduced uptake of the two probes targeting those molecular processes. D20 biodistribution was not impacted by tumor heterogeneity between groups, likely a result of the enhanced permeability and endocytosis of the D20 nanoparticle[17]. Future studies examining tumor-specific probe uptake can account for these biological differences by using greater sample sizes per group based on an appropriate power analysis.

In conclusion, this study demonstrates the feasibility of RO injections for successful systemic delivery of multiple categories of distinct radiotracers. The findings of this study will enable researchers to conduct faster, equally effective, and less invasive RO injections instead of resorting to other, more difficult or invasive approaches for intravenous radiotracer administration. Additionally, these outcomes have the potential for broader applications in intravenous drug delivery methods for research beyond the scope of molecular imaging, given our demonstration of the efficient RO delivery of various commonly used pharmaceutical compounds.

Data availability

The datasets generated during and/or analyzed during the current study are available from the corresponding author on reasonable request.

References

1. James, M. L. & Gambhir, S. S. A molecular imaging primer: Modalities, imaging agents, and applications. *Physiol. Rev.* **92**(2), 897–965. https://doi.org/10.1152/physrev.00049.2010 (2012).
2. Mulero, F., Donate, L. E. & Serrano, M. Imaging cancer in mice by PET, CT, and combined PET-CT. *Curr. Protocols Mouse Biol.* **1**(1), 85–103. https://doi.org/10.1002/9780470942390.mo100137 (2011).
3. Prathipati, P. *et al.* A retrospective analysis for different routes of administration in mice-percutaneous retro-orbital, jugular catheter, tail vein and femoral cut down injections. *J. Biosci. Med.* **8**, 131–141. https://doi.org/10.4236/jbm.2020.89011 (2020).
4. Socher, M., Kuntz, J., Sawall, S., Bartling, S. & Kachelrieß, M. The retrobulbar sinus is superior to the lateral tail vein for the injection of contrast media in small animal cardiac imaging. *Lab. Anim.* **48**(2), 105–113. https://doi.org/10.1177/0023677213517500 (2014).
5. Kienstra, K. A., Freysdottir, D., Gonzales, N. M. & Hirschi, K. K. Murine neonatal intravascular injections: Modeling newborn disease. *J. Am. Assoc. Lab. Anim. Sci.* **46**(6), 50–54 (2007).
6. Lasnon, C., Dugué, A. E., Briand, M., Dutoit, S. & Aide, N. Quantifying and correcting for tail vein extravasation in small animal PET scans in cancer research: Is there an impact on therapy assessment?. *EJNMMI Res.* **5**(1), 61. https://doi.org/10.1186/s13550-015-0141-z (2015).
7. Nanni, C. *et al.* Retro-orbital injection is an effective route for radiopharmaceutical administration in mice during small-animal PET studies. *Nucl. Med. Commun.* **28**(7), 547–553. https://doi.org/10.1097/MNM.0b013e3281fbd42b (2007).
8. Schoch, A., Thorey, I. S., Engert, J., Winter, G. & Emrich, T. Comparison of the lateral tail vein and the retro-orbital venous sinus routes of antibody administration in pharmacokinetic studies. *Lab. Anim. (N.Y.)* **43**(3), 95–99. https://doi.org/10.1038/laban.481 (2014).
9. Steel, C. D., Stephens, A. L., Hahto, S. M., Singletary, S. J. & Ciavarra, R. P. Comparison of the lateral tail vein and the retro-orbital venous sinus as routes of intravenous drug delivery in a transgenic mouse model. *Lab. Anim. (N.Y.)* **37**(1), 26–32. https://doi.org/10.1038/laban0108-26 (2008).
10. Li, S. *et al.* Retro-orbital injection of FITC-dextran is an effective and economical method for observing mouse retinal vessels. *Mol. Vis.* **17**, 3566–3573 (2011).
11. Gomes Marin, J. F. *et al.* Theranostics in nuclear medicine: Emerging and re-emerging integrated imaging and therapies in the era of precision oncology. *RadioGraphics* **40**(6), 1715–1740. https://doi.org/10.1148/rg.2020200021 (2020).
12. Desai, P. *et al.* Radiolabeled nanocarriers as theranostics—Advancement from peptides to nanocarriers. *Small* **18**(25), 2200673. https://doi.org/10.1002/smll.202200673 (2022).
13. Hedhli, J. *et al.* Synthesis, chemical characterization and multiscale biological evaluation of a dimeric-cRGD peptide for targeted imaging of αVβ3 integrin activity. *Sci. Rep.* **7**(1), 3185. https://doi.org/10.1038/s41598-017-03224-8 (2017).
14. Applegate, C. C. *et al.* Impact of administration route on nanocarrier biodistribution in a murine colitis model. *J. Exp. Nanosci.* **17**(1), 599–616. https://doi.org/10.1080/17458080.2022.2134563 (2022).
15. Li, X. *et al.* New frontiers in molecular imaging using peptide-based radiopharmaceuticals for prostate cancer. Review. *Front. Chem.* https://doi.org/10.3389/fchem.2020.583309 (2020).
16. Deng, H. *et al.* Multimodal nanocarrier probes reveal superior biodistribution quantification by isotopic analysis over fluorescence. *ACS Nano* **14**(1), 509–523. https://doi.org/10.1021/acsnano.9b06504 (2020).
17. Sagnella, S. M. *et al.* Dextran-based doxorubicin nanocarriers with improved tumor penetration. *Biomacromolecules* **15**(1), 262–275. https://doi.org/10.1021/bm401526d (2014).
18. Bray, F. *et al.* Global cancer statistics 2022: GLOBOCAN estimates of incidence and mortality worldwide for 36 cancers in 185 countries. *CA Cancer J. Clin.* **74**(3), 229–263. https://doi.org/10.3322/caac.21834 (2024).
19. Mancini, M. *et al.* Head and neck veins of the mouse. A magnetic resonance, micro computed tomography and high frequency color doppler ultrasound study. *PLoS One* **10**(6), e0129912. https://doi.org/10.1371/journal.pone.0129912 (2015).
20. Kreissl, M. C. *et al.* Noninvasive measurement of cardiovascular function in mice with high-temporal-resolution small-animal PET. *J. Nucl. Med.* **47**(6), 974–980 (2006).
21. Jans, H.-S. *et al.* Positron emission tomography (PET) and pharmacokinetics: Classical blood sampling versus image-derived analysis of [18F]FAZA and [18F]FDG in a murine tumor bearing model. *J. Pharm. Pharm. Sci.* **21**(1s), 32s–47s. https://doi.org/10.18433/jpps29788 (2018).
22. Wang, F., Nojima, M., Inoue, Y., Ohtomo, K. & Kiryu, S. Assessment of MRI contrast agent kinetics via retro-orbital injection in mice: Comparison with tail vein injection. *PLoS One* **10**(6), e0129326. https://doi.org/10.1371/journal.pone.0129326 (2015).
23. Yardeni, T., Eckhaus, M., Morris, H. D., Huizing, M. & Hoogstraten-Miller, S. Retro-orbital injections in mice. *Lab. Anim. (N.Y.)* **40**(5), 155–160. https://doi.org/10.1038/laban0511-155 (2011).

Author contributions

All authors contributed to the study conception and design. Material preparation was performed by Yuxiao Cui, data collection and analysis were performed by Catherine C. Applegate, Michael B. Nelappana, Elaine A. Nielsen, Goodluck Okoro, and Nicolas P. Dovalovsky. The first draft of the manuscript was written by Catherine C. Applegate and all authors commented on previous versions of the manuscript. All authors read and approved the final manuscript.

Competing interests

The authors declare no competing interests.

Ethics approval

All animal procedures were approved by the Institutional Animal Care and Use Committee (IACUC) at the University of Illinois at Urbana-Champaign, and all procedures were carried out in accordance with both IACUC guidelines and the ARRIVE guidelines for vertebrate animal experiments.

Additional information

Supplementary Information The online version contains supplementary material available at https://doi.org/10.1038/s41598-024-71221-9.

Correspondence and requests for materials should be addressed to C.C.A.

Reprints and permissions information is available at www.nature.com/reprints.

Publisher's note Springer Nature remains neutral with regard to jurisdictional claims in published maps and institutional affiliations.